General Disclaimer

One or more of the Following Statements may affect this Document

- This document has been reproduced from the best copy furnished by the organizational source. It is being released in the interest of making available as much information as possible.

- This document may contain data, which exceeds the sheet parameters. It was furnished in this condition by the organizational source and is the best copy available.

- This document may contain tone-on-tone or color graphs, charts and/or pictures, which have been reproduced in black and white.

- This document is paginated as submitted by the original source.

- Portions of this document are not fully legible due to the historical nature of some of the material. However, it is the best reproduction available from the original submission.

JPL PUBLICATION 85-12

Microwave Responses of the Western North Atlantic

J.M. Stacey
M.A. Girard

February 15, 1985

NASA
National Aeronautics and
Space Administration

Jet Propulsion Laboratory
California Institute of Technology
Pasadena, California

JPL PUBLICATION 85-12

Microwave Responses of the Western North Atlantic

J.M. Stacey
M.A. Girard

February 15, 1985

NASA
National Aeronautics and
Space Administration

Jet Propulsion Laboratory
California Institute of Technology
Pasadena, California

The research described in this publication was carried out by the Jet Propulsion Laboratory, California Institute of Technology, under a contract with the National Aeronautics and Space Administration.

ABSTRACT

Features and objects in the Western North Atlantic Ocean - the Eastern Seaboard of the United States - are observed from Earth orbit by passive microwaves. The intensities of their radiated flux signatures are measured and displayed in color as a microwave flux image.

The features of flux-emitting objects such as the course of the Gulf Stream and the occurrence of cold eddies near the Gulf Stream are identified by contoured patterns of relative flux intensities.

The flux signatures of ships and their wakes are displayed and discussed. Metal data buoys and aircraft are detected.

Signal-to-clutter ratios and probabilities of detection are computed from their measured irradiances. Theoretical models and the range equations that explain passive microwave detection using the irradiances of natural sources are summarized.

TABLE OF CONTENTS

Figures

Table

The Western North Atlantic Ocean -- the Eastern Seaboard of the United States to a distance of 800 kilometers from the shore -- is a seawater region and the subject of our microwave image.

It's a busy place, day or night, and at any season of the year.

Strong ocean currents, thrusting from the north to the south and at the same time from the south to the north, continually change the water patterns and water features as they interact with each other.

The sometimes strong, and always cold, Labrador current presses southwestward down the coastline from Newfoundland and Nova Scotia, and chills the water along the continental shelf near Cape Cod, Long Island, Delaware, and as far south as Cape Charles, at the entrance to the Chesapeake.

Entering from the Gulf of Mexico, the Gulf Stream rounds the tip of Florida and flows northward along the coasts of Alabama, Georgia, and the Carolinas. As the warm Gulf Stream moves northeasterly, it interacts with the cold shelf water along the coast and with the Labrador current itself, producing eddies and swirls that seem to attach themselves to the west wall of the Gulf Stream and are carried along with it.

In the region to the south of Newfoundland, the Gulf Stream sometimes executes a meandering pattern with hairpin turns. When the direction of the hairpin curves to the south, the cold water from the Labrador Sea enters and fills the hairpin. Later, the bore of the Gulf Stream changes its direction and causes the volume of water that is circulating within the hairpin to be pinched off and cast aside as an autonomous body (an eddy) . . . known as a "cold ring." Cold rings drift in a direction counter to the bore of the Gulf Stream, on its south side. Ultimately, cold rings vanish near the Carolinas.

To the east, and spanning a wide front, is the Sargasso Sea, a huge circulating mass of warm water.

Near Florida are the Bahamas. The water that surrounds them is clear, shallow, and very warm. Between the Bahamas and the Florida coast lies the corridor of the Gulf Stream as it emerges from the Gulf of Mexico and plies northward. Intervening between the Bahamas and the Sargasso Sea is a region of relatively cool water.

There are ships -- small ships, large ships, huge ships -- hundreds of them at any one time. Submarines, as well, operate in the shallow waters of the continental shelf.

Aircraft of all types and sizes abound: cargo planes, intercontinental carriers, and small shuttle planes to the islands.

Large buoys are moored in permanent locations at distances from 70 to 700 kilometers from the coast. Six or more are continually in service. Data buoys measure important meteorological and oceanographic parameters.

Large buoys are Discus-type buoys. That is, their configurations are, as the name implies, disks, with diameters ranging from 6 to 12 meters.

Some buoys look like rectangular boats. They are metal, and their dimensions range from 6 to 8 meters. They are called Boat buoys.

Buoys, aircraft, ships, and submarines comprise the man-made population of the Western North Atlantic.

SECTION I

THE MICROWAVE FLUX MAP

The microwave flux emittances of water features and man-made (metal) objects in the Western North Atlantic are observed and imaged by an Earth-orbiting microwave receiving system with an articulating, collecting aperture. The scene of observation and the microwave imagery are shown in Figure 1.

The imaged parameter for emitting objects is the relative flux intensity (watts) produced by thermal gradients in the surface features. For metal objects, the imaged parameter is the relative flux produced by the bistatic gain properties of the metallic objects, as they redirect the downwelling irradiances of the atmosphere and the cosmic background into the articulating, collecting aperture on the spacecraft.

The projection given by the microwave flux is a Mercator. The coordinates are north latitude and west longitude. The width and length dimensions are 718 and 2400 kilometers, respectively. The colors represent orders of flux intensity. In ascending order, they are, from left to right:

pink

red

yellow

gold

green

light blue

medium blue

lavender

violet

dark blue

Figure 1.a. The Western North Atlantic (annotated color code)

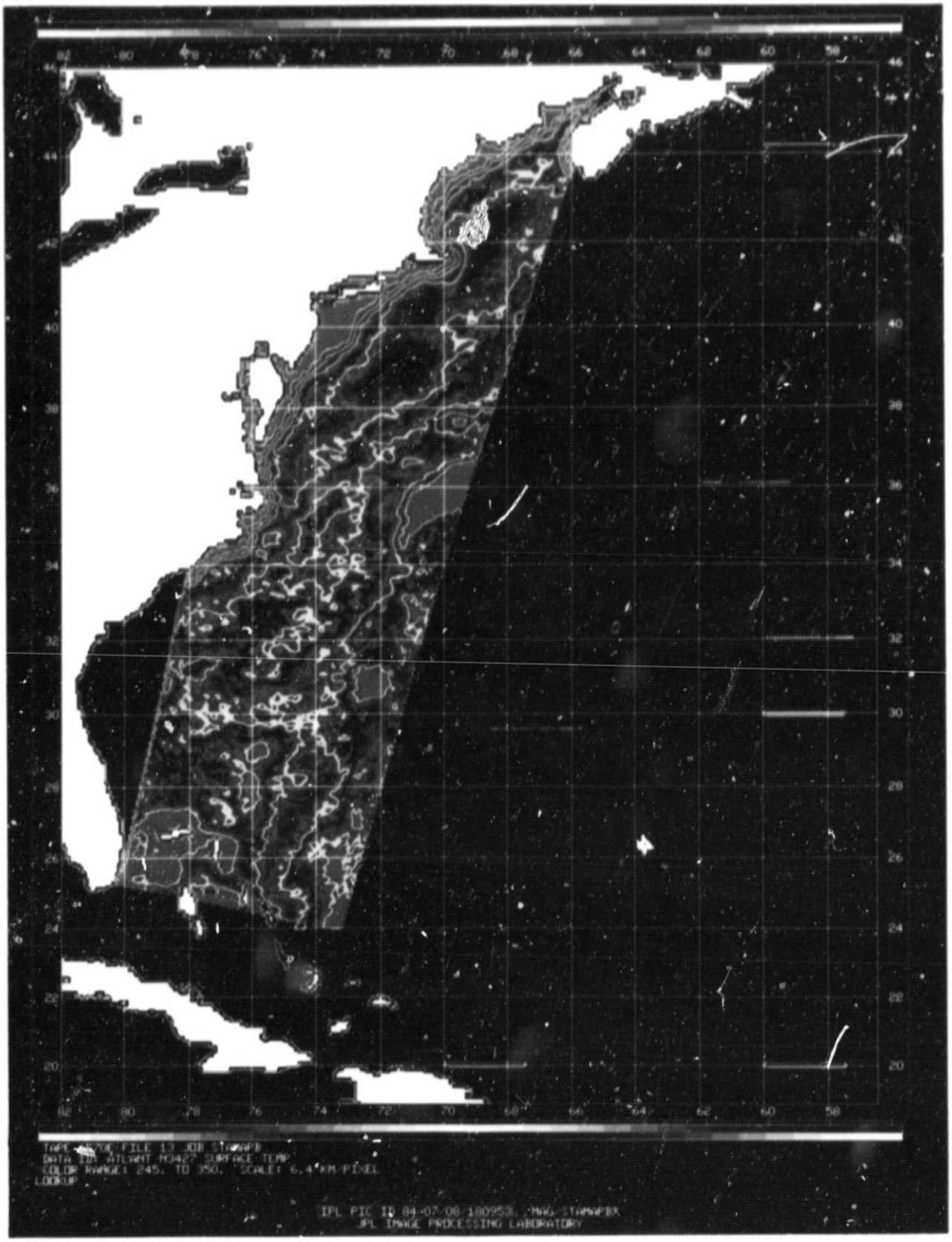

Figure 1.b. The Western North Atlantic (a microwave flux image)

Figure 1.c. The Western North Atlantic

Because of the wide dynamic range of flux intensities in the image, the color code replicates. That is, for flux intensities that exceed that of the pink, the colors start again with dark blue. Similarly, for flux intensities that are lower than that of the dark blue, the color code sequences in reverse, starting with pink. By expectation, the replicating colors produce ambiguities at particular flux levels.

The color code operates independently for emitting objects and for metal objects. Because the processes that determine the flux intensities for emitting objects and metal objects are different, their replicating colors are uncorrelated.

A. THE GULF STREAM

The west wall of the Gulf Stream is shown in colored isofluxes. From 33 (north latitude)/78 (west longitude), medium- and light-blue isoflux lines clearly delineate the serpentine course of the Gulf Stream to where it exits the image at 39/68. Also, mainly in yellow and red, the west wall of the Gulf Stream is seen to meander northeastward where it interacts with several thermal attachments along the way; one attachment in particular at 40/69.5 exhibits the characteristics of a small, warm eddy.

A concurrent infrared image of the Gulf Stream is displayed for comparison in shades of black and white in Figure 2. The infrared and the microwave observations were taken within a few hours of each other. At the lower-center edge of the infrared image, the bore of the Gulf Stream enters, where it is viewed in dark shades that signify warm temperatures. White shades signify colder temperatures. In the infrared image, the bore of the Gulf Stream passes to the south of Cape Hatteras, as it commences its

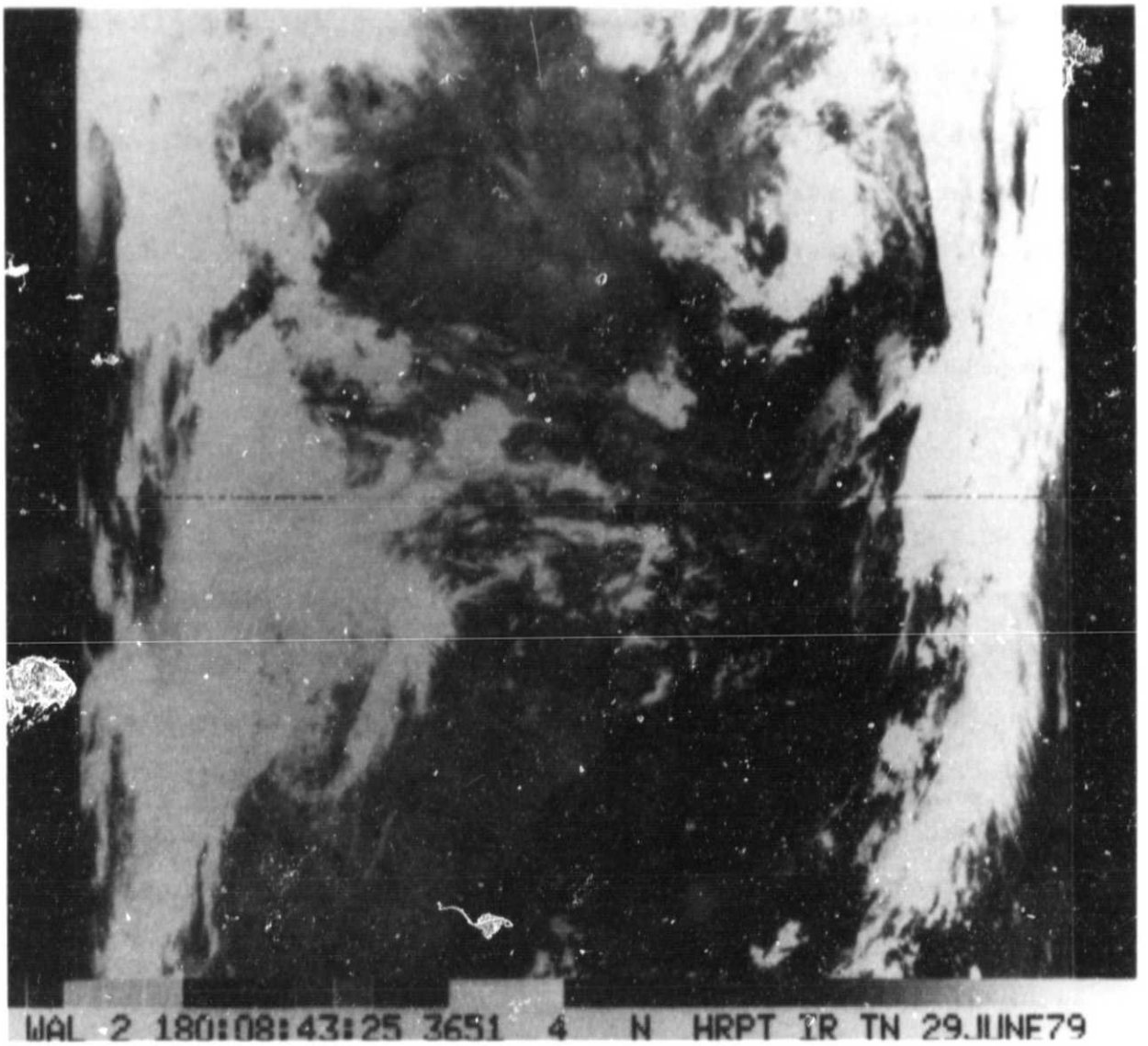

Figure 2. An infrared image of the bore of the Gulf Stream, near and south of Cape Hatteras, on June 29, 1979 at 0843 hours Universal time. The bore is shown in dark shades. Cumulus cloudforms are shown in shades of white. Lake Erie is barely perceptible in the upper-left corner. The infrared and microwave flux images were taken within a few hours of each other.

northeasterly course. To the east of Cape Hatteras, the Gulf Stream disappears under a cumulus cloud.

An overcast of intermittent cumulus clouds characterizes the general weather pattern during the time of the observation. Precipitating clouds are shown in red and pink as they occur over the Sargasso Sea near 36/70 and again near Long Island and New Jersey at 40/73.5. Cloud patterns and areas of precipitation are identified in the infrared images that are taken at the same time as the microwave flux observations. (See Figure 3.)

B. METAL OBJECTS

The flux signatures (passive measurements) of many metal objects appear in the image. The strength (signal-to-clutter ratio, S/C) and the probability of detection, P_d, are computed for several objects. The criteria for estimating signal-to-clutter ratios and probabilities of detection are discussed under "Detectability Criteria."

The identification of the metal objects shown in the image is based on experience. A large number of observations and measurements of metal objects were taken from orbit during planned experiments in the Gulf of Alaska during 1978. Ships, aircraft, and buoys participated in the experiment -- they were particularly identified and positioned within the view of the microwave flux imager for many overpasses of the spacecraft (Seasat). Some objects were observed more than once.

From these controlled experiments the signatures of ships, wakes, aircraft, and buoys were identified and analyzed. A partial listing of the metal objects observed during these experiments is given in Table 1.

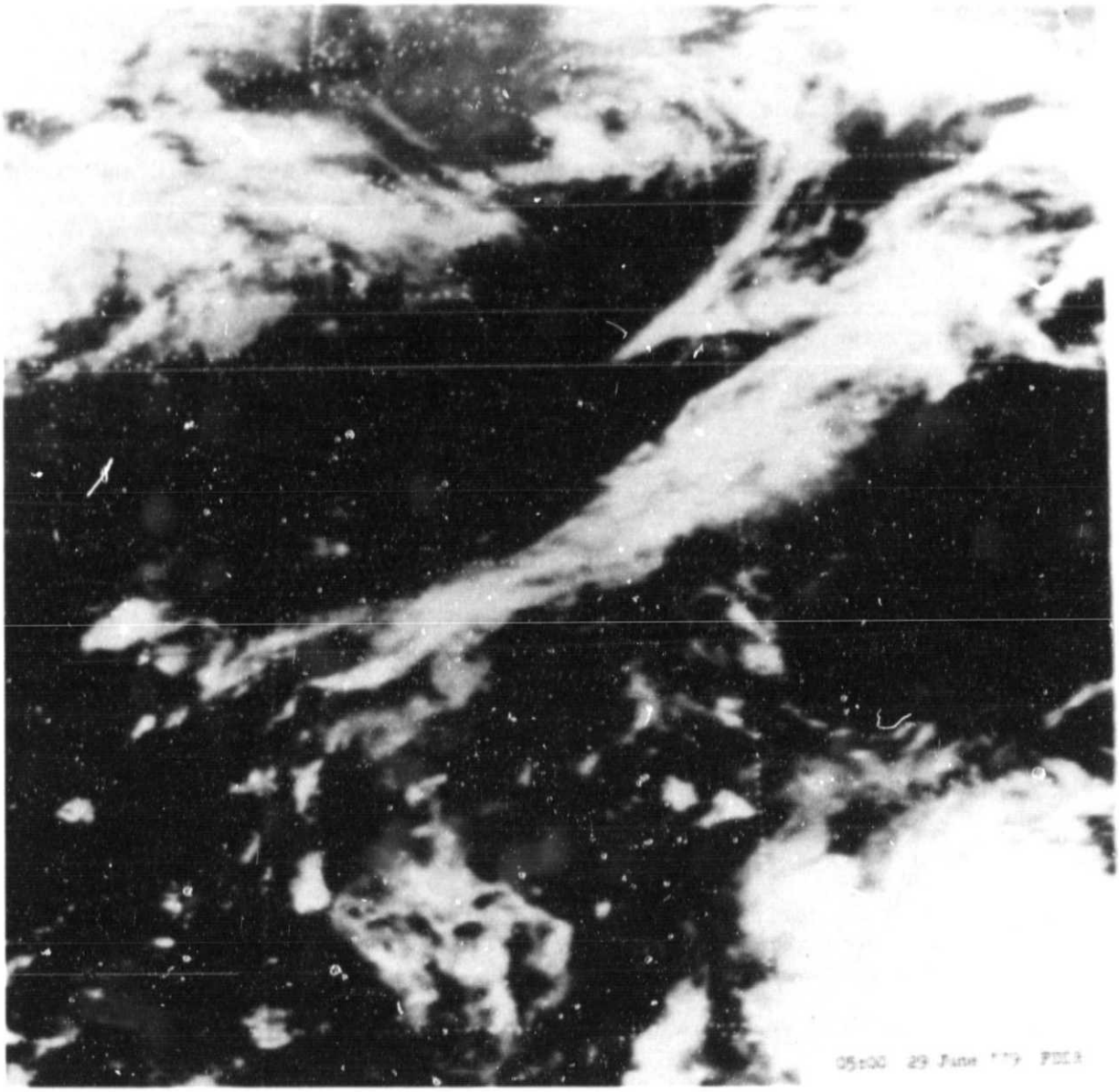

Figure 3. The Western North Atlantic -- an infrared image by NOAA on June 29, 1979 at 0500 hours Universal time. The southeast coast of the United States is shown with the Western North Atlantic region. Shades of white are cumulus clouds. Alabama and South Carolina are essentially cloud free. Lake Erie is perceptible in the upper left corner. Coordinates intersecting near northern Florida are 30N/80W. The Gulf Stream is not visible in this large area image.

Table 1. Metal objects detected from Earth orbit
(Microwave Flux Measurements)

	S	C	(S/C)dB	P_d	ORBIT Id.
ASTRODOME SITES					
Mt. Hopkins	20.25	1.23	12.63	0.69	/480/
Mt. Hopkins	5.64	1.23	6.6	0.27	/344/
Palomar	20.69	1.30	13.16	0.72	/480/
Jungfraujoch	25.93	5.53	6.71	0.28	/196/
Zermatt	25.55	2.05	10.96	0.58	/196/
Sonneberg	23.86	2.14	10.47	0.53	/196/
ANTENNA SITES					
Kitt Peak (11 m)	43.90	1.44	14.78	0.79	/480/
Kitt Peak (11 m)	66.55	4.20	11.99	0.65	/344/
DSN Canberra (85 m)	21.39	5.10	6.23	0.25	/355/
Parkes (64 m)	12.23	3.93	5.27	0.19	/355/
Owens Valley (40 m)	28.32	4.16	8.33	0.40	/531/
Hat Creek (26 m)	7.17	3.80	8.56	0.41	/531/
Yebes Station (4 m)	25.34	2.70	9.73	0.50	/871/
Bonn (100 m)	15.08	2.53	7.75	0.35	/196/
AIRCRAFT					
CV-990	37.96	2.87	11.21	0.60	/1163/
RP-3A	31.95	1.30	13.89	0.75	/1212/
CV-580	38.47	3.90	9.86	0.51	/1292/
SPACECRAFT					
NOAA-C	64.91	3.76	12.37	0.67	/N20733/
NOAA-C	27.62	4.88	7.53	0.34	/N21012/
SHIPS					
Oceanographer	30.00	2.04	11.67	0.63	/1163/
Oceanographer	13.22	3.53	5.73	0.22	/934/
Oceanographer	163.06	3.38	16.97	0.87	/1212/
Oceanographer*	10.90	2.46	4.44	0.26	/1292/
Oceanographer	30.00	3.91	8.85	0.43	/940/
Oceanographer	8.90	3.72	3.79	0.12	/1006/
Merchant Ship (CGBS)	20.75	1.53	11.32	0.61	/1163/
Merchant Ship (5LGP)	24.00	8.40	2.86	0.15	/1292/
Merchant Ship (WLDF)	23.71	4.68	5.07	0.30	/1292/
Vancouver	28.60	5.83	6.91	0.29	/934/
Vancouver	12.81	4.51	4.53	0.15	/940/
Vancouver	9.34	4.32	3.35	0.10	/1006/
BUOYS					
46001 (12 m)	25.52	4.49	7.55	0.34	/1006/
46004 (12 m)	18.29	2.32	8.97	0.44	/934/
46004 (12 m)	26.10	3.54	8.67	0.42	/1212/
46004 (10 m)	16.50	1.04	12.00	0.65	/466/
46005 (12 m)	27.16	2.44	10.46	0.55	/1212/

*Raining Clouds

Table 1. Metal objects detected from Earth orbit
(Microwave Flux Measurements) (continued)

BUOYS (continued)		S	C	(S/C)dB	P_d	ORBIT Id.
46005	(10 m)	28.81	2.73	10.24	0.54	/466/
46006	(12 m)	24.28	3.95	7.88	0.36	/940/
46008	(6 m)	9.74	5.01	2.88	0.09	/940/
44002	(6 m)*	13.58	5.04	4.30	0.14	/N3427/
44002	(6 m)	25.22	4.44	7.54	0.34	/888/
44003	(6 m)	30.86	4.01	8.86	0.44	/N3427/
44005	(12 m)	20.09	3.72	7.32	0.32	/N3427/
44005	(12 m)	28.30	5.42	7.18	0.31	/N1160/
44004	(12 m)	25.84	2.56	10.05	0.52	/888/
44004	(12 m)	38.29	6.33	7.81	0.36	/1017/
44004	(12 m)	42.70	6.03	8.50	0.41	/931/
44002	(6 m)	23.81	2.32	10.12	0.53	/931/
44002	(6 m)	23.06	3.93	7.68	0.35	/1017/
44001	(6 m)	19.87	3.54	7.49	0.34	/N3427/
44001	(6 m)	10.68	3.68	4.63	0.16	/N1160/
44001	(6 m)	25.07	3.64	8.39	0.37	/1017/
42001	(6 m)	27.49	5.49	7.00	0.30	/1440/
41004	(5 m)	17.89	1.11	12.08	0.66	/888/
41004	(5 m)	48.78	4.37	10.48	0.55	/1017/
41002	(10 m)	28.13	2.24	10.98	0.59	/N3427/

LEGEND

S — Signal output of the receiver in digital counts (relative flux units).

C — Temperature-resolution (RMS) clutter magnitude at the output of the receiver in digital counts (relative flux units).

(S/C)dB — Signal-to-clutter power ratio expressed in decibels.

P_d — Calculated probability of detection from the S/C ratio and the probability of a false alarm.

$$P_d = P_n^{1/(1 + S/N)}$$

- Detector threshold level: one false alarm for 1377 independent samples in 60 seconds.
- False alarm probability: P_n = 7.26E-04
- Conforming with the accepted interpretation of the probability of detection for scanning collectors, a probability of detection of 0.5 expresses the expectation that 5 out of every 10 targets having similar statistics would be detected. This interpretation is consistent with, and analogous to, the familiar blip-scan criterion used in radar detection.

*Raining Clouds

Table 1. Metal objects detected from Earth orbit
(Microwave Flux Measurements) (continued)

LEGEND (continued)	
ORBIT Id.	Orbit identifier. When the orbit number is prefixed by the letter N the data are taken from the Nimbus-7 spacecraft receivers. Otherwise, the data are taken from Seasat spacecraft receivers.
GSF	Gain scale factor = 8 (digital counts)/kelvin.
SENSOR	o Microwave flux imager o Articulating collecting aperture = 0.49 m^2 o Operating wavelength = 0.008 meters

In addition to the metal objects participating in the controlled experiments over seawater, Table 1 contains the measured results of some land-based metal objects for the purpose of gaining additional experience in the observation of metal objects as a category. The physical characteristics of the land-based metal objects and their geodetic coordinates are precisely known. For this reason they serve as excellent test targets with surface truth incorporated as an intrinsic feature.

The experience gained by these observations of metal objects, both during planned experiments over seawater and on land sites, serves importantly to provide the interpretation for the signatures shown in the flux image.

C. BUOYS

From north to south:

Buoy 44005 lies between Cape Cod and Nova Scotia at 42.8/68.2. It is a 12-meter diameter Discus type and appears as a medium-blue dot. S/C = 7.3 dB, P_d = 0.32.

Buoy 44003 is moored at 40.7/68.4, southeast of Cape Cod. It is a 6-meter Boat type and appears as a yellow dot.

S/C = 8.9 dB.

Buoy 44001 is moored at 38.6/73.5, southeast of the Delaware River. It is a 6-meter Boat type. Buoy 44001 is not visible in the image because its flux signature is coded with a yellow dot that is superposed on an ambiguous yellow isoflux contour.

S/C = 7.5 dB.

Buoy 41001 is moored at 32.3/75.4, southeast of Cape Hatteras. It is a 6-meter Boat type. It appears as a dot with medium-blue and light-blue shades.

S/C = 10.9 dB, P_d = 0.58.

Buoy 44002 is moored at 40.1/73, about 70 km southeast of New York City. It is a 6-meter Boat type. The region surrounding 44002, is saturated in shades of pink because of the occurrence of raining clouds in the local area. For this reason 44002 is not visible in the image. Rain-cloud attenuation reduces the S/C ratio, as expected. From the digital data record, the S/C is computed for this buoy.

S/C = 4.3 dB.

Figure 4 shows an operational 12-meter Discus buoy, and Figure 5 shows an operational 6-meter Boat buoy.

The scattering cross sections of NOAA data buoys are typically enhanced by corner reflectors.

Buoys are important objects because:

- They are abundantly distributed and have scheduled in situ availability.

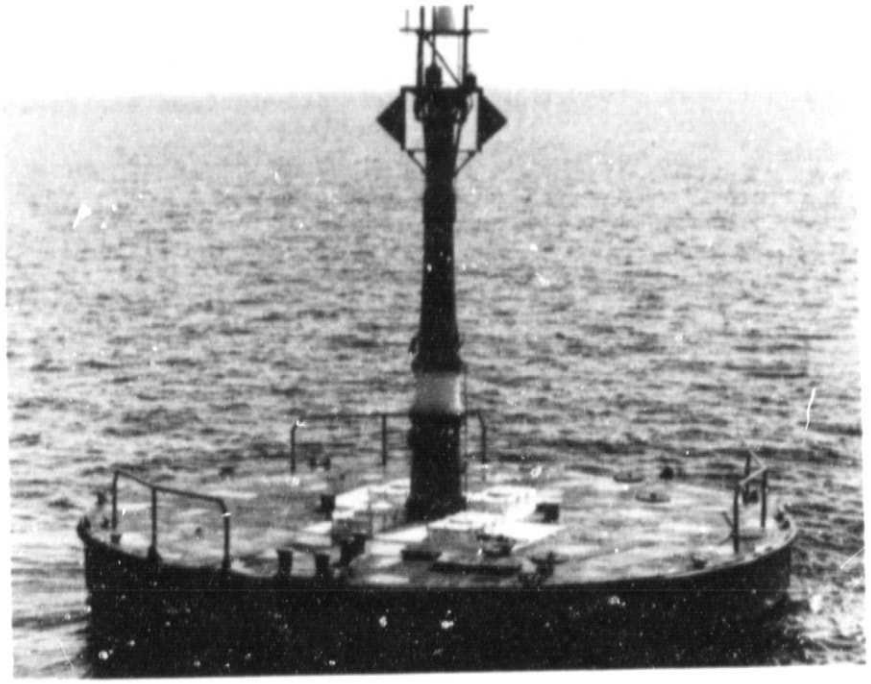

Figure 4. A 12-meter Discus buoy

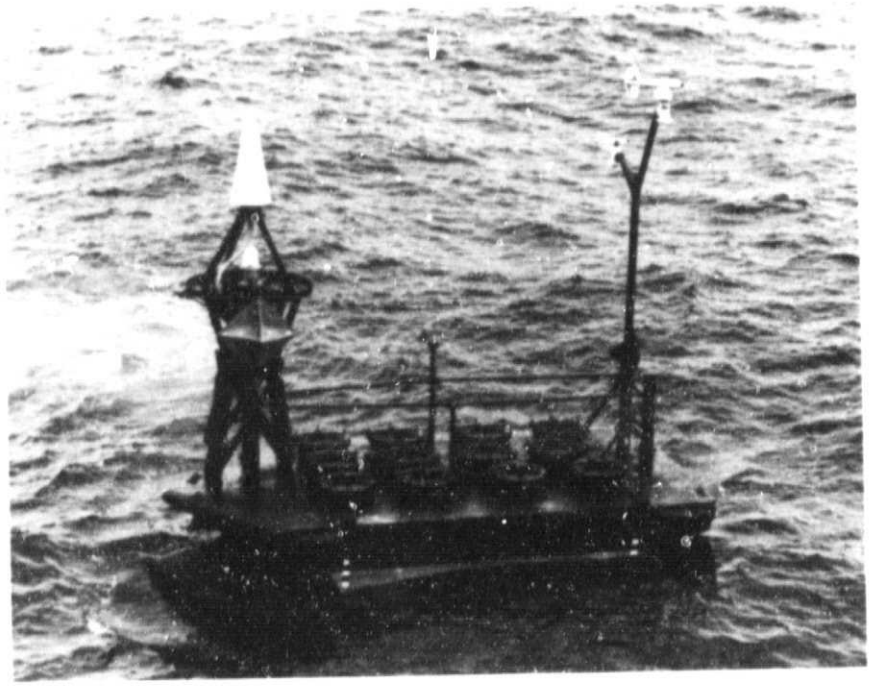

Figure 5. A 6-meter Boat buoy

- They are moored and their coordinates are precisely known.
- They are constructed as simple geometrical figures (disks and rectangles) that produce useful and well-defined scattering properties. The scattering properties of buoys are enhanced by appending corner reflectors.

D. SHIPS AND WAKES

A ship and its wake are identified in the flux image as a uniform colored ribbon with a dot near one end. The ribbon characterizes the wake, and the dot, the ship.

An inspection of the flux image shows many signatures of ships and wakes. For example, within the rectangle bounded by (26 to 28) north latitude/(74 to 76) west longitude are the signatures of several ships and their wakes. Within the same rectangle, and near 28° latitude, a red ship with a yellow wake follows a light-blue ship with a medium-blue wake. Both are on a course of about 100° true. The yellow wake radiates a higher flux level than the green surfaces that surround it. Similarly, the medium-blue wake radiates a higher flux than the adjacent lavender surfaces. The precise coordinates of the light-blue ship are determined and the S/C ratio is computed from the digital data record: 5.5 dB (P_d = 0.20).

Relative flux intensity comparisons between ships and wakes are not permissible with the replicating 10-color code. It is to be emphasized that the signatures and fluxes of emissive objects and metal objects are produced by different phenomena, and they are uncorrelated in the color code.

Immediately to the south of the medium-blue wake, and on a course parallel to it, is another medium-blue wake with a light-blue inner wake. The ship, as a dot, is not apparent in the flux image.

Wakes with higher flux levels than their surrounding surfaces are, typically, characterized by the presence of foam. Foam operates to increase the emissivity of the wake and the level of the flux. The development of the foam pattern for a wake-in-the-making is illustrated in Figure 6.

Ships that are underway, with no way on, or ships that are moving slowly produce little foam, and their wakes radiate a lower flux level than the adjacent medium.

Within the rectangle bounded by (42 to 44)/(66 to 48) are several ships with wake fluxes that are lower than the surrounding media. The wakes are shown in light blue. The ships are shaded with a medium blue. The surrounding media are shaded in green, gold, and yellow, which signify higher flux levels than the wakes. This area is characterized by commercial fishing activities.

Within the rectangle bounded by (32 to 34)/(76 to 78), off the coast of the Carolinas, are examples of several ships (dots) and their ribbon-like wakes.

The ship at 40.3/71.3, departing from the New Jersey/New York City area, bearing 090° true, appears to be extremely large . . . judging from the size of the wide wake and the elongated representation for the ship. The S/C ratio was computed for this ship from the digital record: 2.44 dB (P_d = 0.07). Because of the near proximity of the ship to the land, the magnitude of the clutter entering the sidelobes is high, and for this reason, the S/C ratio is smaller than expected.

Figure 6. Wake and foam pattern produced by a fishing boat at 12 knots. Width of the stern is 6 meters. San Clemente Island is in the background.

E. AIRCRAFT

Aircraft signatures appear in the flux image as colored dots. They are easily distinguished from ships because there is no evidence of a wake.

Aircraft signatures are ambiguous with the signatures of buoys. The ambiguity is easily resolved, however, because the locations of moored buoys are precisely known.

The ambiguity between an aircraft and a ship that produces no detectable wake can sometimes be resolved. That is, a ship at anchor, or one that is underway with no way on would not be expected to produce a wake. Frequently, however, a wake is produced by the interaction of the ship's hull with the movements of local currents.

Sometimes buoys produce wakes. When strong local currents drive a buoy against its tether, a smooth wake is produced for a short distance behind. Because of the absence of foam, a smooth wake will produce a lower flux level than the adjacent water.

Experience, and familiarity with the interpretation of the features in the flux image, are enormously important for resolving signature ambiguities.

From the flux image, three aircraft are identified from their signatures:

- At 42.2/68.5, a blue dot, northeast of Cape Cod. From the digital data record the S/C ratio is computed:

  S/C = 7.5 dB, P_d = 0.34.

- At 39.1/71.8, a violet dot, southeast of Long Island.

  S/C = 10.5 dB.

- At 26.7/75.3, a medium-blue dot, east of the Bahamas.

  S/C = 10.8 dB, P_d = 0.57.

Other candidate aircraft signatures are identifiable in the image.

Without concurrent surface truth or previous information there is always the risk of error in the identification of aircraft. Again, risks reduce as experience increases.

Aircraft in the region of the Western North Atlantic Ocean can be expected to operate well above the attenuating effects of clouds and other attenuating media. For this reason the metal surfaces of the aircraft are fully exposed to the irradiance of the cosmic background, and the reradiated flux levels produce signal-to-noise ratios that portend useful probabilities of detection even with relatively small collecting apertures operating in Earth orbit.

Comparisons between the S/C ratios for aircraft and buoys are interesting and relevant -- especially, as relative detectability is affected. The bistatic, scattering cross sections of buoys are enhanced because of their symmetrical geometry and because they sometimes incorporate corner reflectors to improve detectability. Buoy detectability suffers the attenuating effects of rain in the downwelling and upwelling paths through the atmosphere.

The physical areas of the reflecting surfaces of commercial aircraft are larger than buoys. Typically, commercial aircraft expose hundreds of square meters of metal surface on their topsides. The largest Discus-type buoys expose less than 115 m^2. The reflecting surfaces of aircraft functionally operate as an ensemble of random scatterers where only a small fraction of the aircraft area participates in the bistatic scattering process. Per contra, buoys possess a basic symmetrical figure that causes more of the scattering surfaces to participate; the scattering coefficients are greater than for aircraft. For this reason the scattering cross sections for buoys and aircraft are quite similar.

F. THERMAL FEATURES AND CLOUDS

Raining cloudforms appear as small areas that are saturated in pink. Three of them are particularly noticeable:

- 40/73.5, near the New Jersey coast.
- 36/70, at the eastern perimeter of the image and extending into the Sargasso Sea.
- 31/72.3, also near the eastern perimeter of the image in the Sargasso Sea.

Rain cloudforms, in the Western North Atlantic, usually occur over a small area; typically, they are less than 100 km in diameter. Widespread precipitation is rare . . . at least, insofar as it is detectable by microwave flux. Raining clouds produce rain within their own volume. As viewed from orbit it is unclear when, or if, the water particulates formed in rain clouds ever reach the surface.

Cloud coverage for a portion of the Western North Atlantic is shown in the infrared image, Figure 3. The infrared and microwave images were taken within the same hour. Microwave flux penetrates nonraining cloudforms with low attenuation losses as compared to visible and infrared wavelengths. There is no evidence of the cumulus cloudforms shown in the infrared in Figures 2 and 3 in the microwave flux image (Figure 1).

Flux levels increase when the central response of the collecting aperture or some of the sidelobes interact with the shore and the land. The steep rise in flux caused by the shore is shown by the closely packed color contours along the coast from the Carolinas to Nova Scotia. High flux levels from the land saturate in pink.

The clear shallow water surrounding the Bahamas is very warm; it radiates high flux levels that are shown in pink.

SECTION II

DETECTABILITY CRITERIA

The detection capability of the receiver for emitting objects on the surface is specified by the flux density (radiant emittance) of a Lambertian Disk Emitter whose diameter is 1640 meters and whose temperature difference, with respect to the Earth's background temperature, is 2 kelvins.

The irradiance of the Lambertian Disk Emitter arrives in the wavefront at the collecting aperture after transiting a slant range of 1000 km. At this slant range, the irradiance is sufficient to produce a 10-dB signal-to-noise (S/N) ratio.

The model and the range equations that explain the detection capability for emissive objects are derived from first principles, and the results are summarized in Figure 7.

The detection capability of the receiver for metal objects is specified by the flux density (radiant emittance) scattered by a metallic surface whose scattering area is 158 m^2, which is further modified (reduced) by a reflectivity factor of 0.06 (-12.2 dB).

The scattered flux from the metal object arrives at the collecting aperture after transiting a slant range of 1000 km. At this slant range, the collected irradiance is sufficient to produce a 10-dB S/N ratio.

The model and the range equations that explain the detection capability for metal objects are derived from first principles, and the results are summarized in Figure 8.

The N term, in S/N, is an orthogonal average (root sum of squares) of the receiver noise power and the clutter power that arrives at, and is referenced to, the phase center of the collecting aperture. Typically, in this receiving

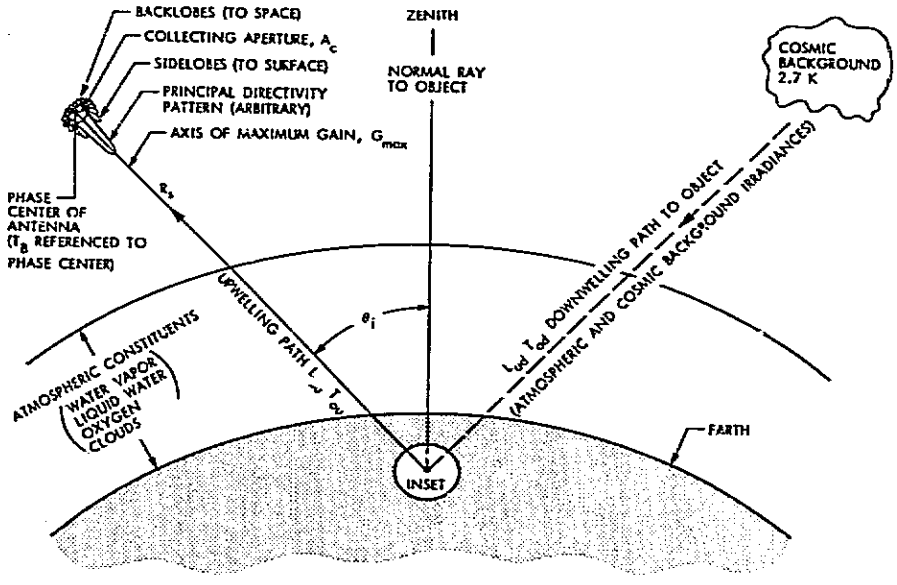

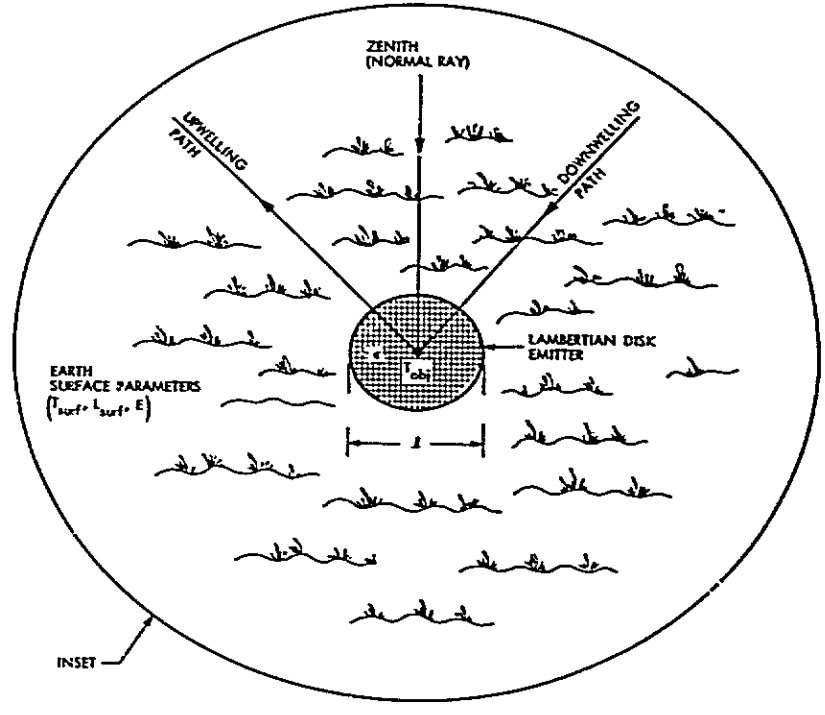

LEGEND

T_{ou} = INTEGRATED PHYSICAL TEMPERATURE OF THE UPWELLING PATH, K

L_{ou} = LOSS IN THE UPWELLING PATH

T_{surf} = PHYSICAL TEMPERATURE OF THE SURFACE MATERIAL, K

L_{surf} = LOSS IN THE SURFACE MATERIAL

T_{od} = INTEGRATED PHYSICAL TEMPERATURE OF THE DOWNWELLING PATH, K

L_{od} = LOSS DOWNWELLING PATH, K

T_B = THERMODYNAMIC TEMPERATURE OF THE BACKGROUND, K

T_{obj} = TEMPERATURE OF OBJECT (UNIFORM), K

ϵ = EMISSIVITY OF OBJECT

ℓ = DIAMETER OF OBJECT, m

R_s = SLANT RANGE (COLLECTING APERTURE TO OBJECT), m

A_c = AREA OF COLLECTING APERTURE, m^2

G_{max} = AXIS OF MAXIMUM ANTENNA GAIN

θ_i = INCIDENCE ANGLE, deg

$$T_B = \underbrace{\frac{T_{cosmic}}{L_{od}\,L_{surf}\,L_{ou}}}_{[\text{COSMIC}]} + \underbrace{\frac{T_{od}\,(L_{od}-1)}{L_{od}\,L_{surf}\,L_{ou}}}_{[\text{DOWNWELLING}]} + \underbrace{\frac{T_{surf}\,(L_{surf}-1)}{L_{surf}\,L_{ou}}}_{[\text{SURFACE}]} + \underbrace{\frac{T_{ou}\,(L_{ou}-1)}{L_{ou}}}_{[\text{UPWELLING}]},\ K$$

WHERE: E = EMISSIVITY

$$L_{surf} = \frac{1}{1-E}$$

SUBCRIPTED L SYMBOLS ARE DISSIPATIVE LOSSES EXPRESSED AS A NUMBER > 1.

Figure 7.a. Theoretical model for emitting objects as observed from orbit.

$$(S/N) = \frac{\pi \sigma \epsilon \cos \theta_i T^4 \ell^2 (A_c \eta)}{4\left(4\pi R_S^2\right) L_{au} k T' B}, \quad \text{DIMENSIONLESS} \qquad (11a)$$

$$(S/N) = \frac{2.57 \times 10^{14} \epsilon \cos \theta_i T^4 \ell^2 (A_c \eta)}{R_S^2 T' B L_{au}}$$

WHERE

σ = 5.67032E+08 STEFAN-BOLTZMANN CONSTANT.

ϵ = EMISSIVITY OF EMITTING OBJECT (NORMAL INCIDENCE).

θ_i = ANGLE OF INCIDENCE, DEG.

T = DIFFERENCE TEMPERATURE: EMITTING OBJECT TEMPERATURE MINUS THE BACKGROUND TEMPERATURE $|T_{obj} - T_B|$, K

ℓ = DIAMETER OF EMITTING OBJECT, m

A_c = AREA OF COLLECTING APERTURE, m^2

η = SOLID ANGLE MAIN BEAM EFFICIENCY.

R_S = SLANT RANGE, m

L_{au} = ATMOSPHERIC ATTENUATION, A NUMBER > 1.0.

k = 1.380662E-23 BOLTZMANN CONSTANT.

T' = CLUTTER PLUS RECEIVER NOISE, ORTHOGONAL AVERAGE, K

B = PREDETECTION BANDWIDTH, HERTZ

Figure 7.b. Summary of the range equations for emitting objects as observed from orbit. (Ref. 1)

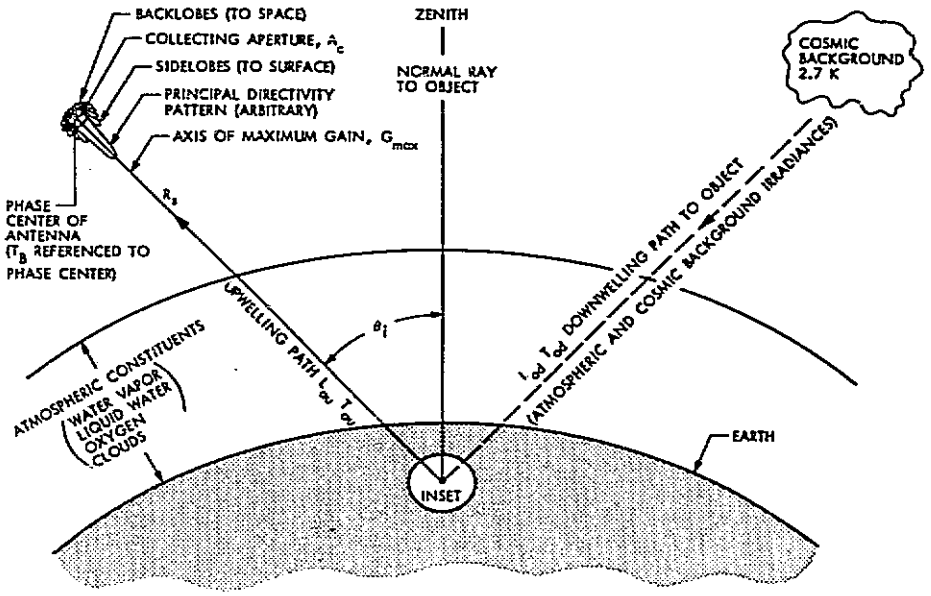

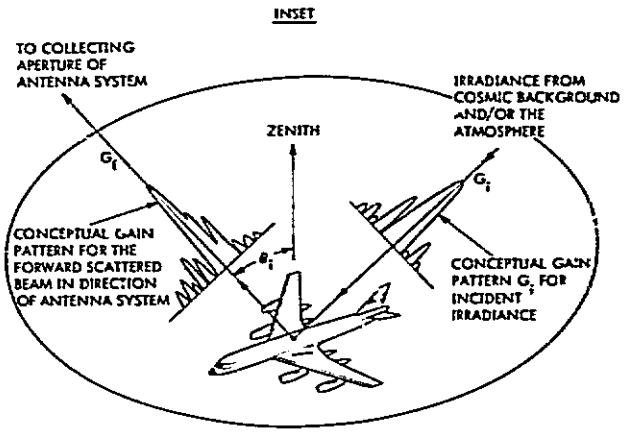

LEGEND

T_{au} = INTEGRATED PHYSICAL TEMPERATURE OF THE UPWELLING PATH, K

L_{au} = LOSS IN THE UPWELLING PATH

T_{surf} = PHYSICAL TEMPERATURE OF THE SURFACE MATERIAL, K

L_{surf} = LOSS IN THE SURFACE MATERIAL

T_{od} = INTEGRATED PHYSICAL TEMPERATURE OF THE DOWNWELLING PATH, K

L_{od} = LOSS DOWNWELLING PATH, K

T_B = THERMODYNAMIC TEMPERATURE OF THE BACKGROUND, K

R_s = SLANT RANGE (COLLECTING APERTURE TO OBJECT), m

A_c = AREA OF COLLECTING APERTURE, m^2

G_{max} = AXIS OF MAXIMUM ANTENNA GAIN

θ_i = INCIDENCE ANGLE, deg

$$T_B = \underbrace{\frac{T_{cosmic}}{L_{od}\,L_{surf}\,L_{au}}}_{[\text{COSMIC}]} + \underbrace{\frac{T_{od}\,(L_{od}-1)}{L_{od}\,L_{surf}\,L_{au}}}_{[\text{DOWNWELLING}]} + \underbrace{\frac{T_{surf}\,(L_{surf}-1)}{L_{surf}\,L_{au}}}_{[\text{SURFACE}]} + \underbrace{\frac{T_{au}\,(L_{au}-1)}{L_{au}}}_{[\text{UPWELLING}]}, \text{K}$$

WHERE: E = EMISSIVITY

$$L_{surf} = \frac{1}{1-E}$$

SUBCRIPTED L SYMBOLS ARE DISSIPATIVE LOSSES EXPRESSED AS A NUMBER > 1.

Figure 8.a. Theoretical model for metal objects as observed from orbit.

$$\frac{S}{N} = \frac{4\pi(T_B - T_{CA})\,(A_T Z_r)^2\,(A_c \epsilon_{sa})}{R_s^2\,\lambda^4\,(T_{clut}^2 + T_R^2)^{1/2}\,L_{au}}\ , \text{ DIMENSIONLESS}$$

WHERE:

T_B = BACKGROUND TEMPERATURE FOR TARGET, K
(<100 K FOR SMOOTH COLD SEAS TO > 300 K FOR TROPICAL FORESTS.)

T_{CA} = EMISSION TEMPERATURE OF THE DOWNWELLING PATH AT THE SURFACE, K
(TYPICALLY 27 K, AT SEA LEVEL, AT MID-LATITUDES, CLEAR DAY, 8-mm WAVELENGH)

A_T = PROJECTED AREA OF TARGET AS VIEWED FROM THE ANTENNA SYSTEM, M^2
(LARGE BUOYS AND AIRCRAFT TYPICALLY RANGE FROM 100 OVER 300 M^2)

Z_r = REFLECTIVITY FACTOR FOR THE TARGET AREA, DIMENSIONLESS
(MEASURED VALUES FOR CERTAIN COMMON AIRCRAFT ARE TYPICALLY 0.06)

A_c = AREA OF THE COLLECTING APERTURE OF THE ANTENNA SYSTEM, M^2)

R_s = SLANT RANGE, TARGET TO ANTENNA SYSTEM, M

ϵ_{sa} = SOLID ANGLE MAIN BEAM EFFICIENCY OF THE ANTENNA, DIMENSIONLESS
(0.6 TO > 0.95 FOR POOR AND EXCELLENT ANTENNA DESIGNS, RESPECTIVELY)

λ = OPERATING WAVELENGTH OF THE ANTENNA SYSTEM, M

T_{clut} = RMS VALUE OF THE CLUTTER COMPONENTS ENTERING THE SIDELOBES
AND BACKLOBES OF THE ANTENNA SYSTEM AND FROM THE BACKGROUND, K
(TYPICAL RANGE: 1 TO 5 K, AS DEDUCED BY ACTUAL EXPERIENCE)

T_R = RMS NOISE LEVEL OF THE ANTENNA SYSTEM RECEIVER, K
(TYPICALLY RANGES FROM 0.5 TO 1.5 K)

L_{au} = ATTENUATION IN THE UPWELLING PATH, DIMENSIONLESS
(A NUMBER > 1, TYPICALLY 1.08 [0.35 dB], AT 8-mm WAVELENGTH,
CLEAR DAY, MID-LATITUDES.)

Figure 8.b. Summary of the range equations for metal objects as observed from orbit. (Ref. 1)

system, the clutter power easily dominates the magnitude of N. For this reason the S/C is used as a preference.

The clutter power is estimated from the RMS variations (standard error of estimate) of the background temperature hyperplane in the local vicinity of the emitting object or metal scatterer.

The single-look probability of detection, P_d, has been computed for several metal objects of interest and has been expressed along with the measured S/C.

P_d is based on the expression

$$P_d = P_n^{1/(1 + S/N)}$$

where P_n is further defined as the false alarm probability and is expressed for this particular receiving system as

$$P_n = \frac{\text{Number of allowable false alarms in time T}}{\text{Number of independent samples in time T}}$$

As an arbitrary criterion for setting the threshold level of the detector, we allow one false alarm every 60 seconds. During this period of time the receiver and the articulating collector produce 1377 independent samples. From this, P_n is estimated by $1/1377 = 7.26 \times 10^{-4}$.

Conforming with the accepted interpretation of the probability of detection for scanning collectors, a probability of detection of 0.5 expresses the expectation that 5 out of every 10 targets having similar statistics would be detected. This interpretation is consistent with, and analogous to, the familiar blip-scan criterion used in radar detection.

SECTION III

THE OBSERVATION

The observation occurred over the Western North Atlantic on June 29, 1979, at 0510 hours Universal time. The receiving system was carried by a Nimbus spacecraft.

The collecting aperture articulates and possesses a physical aperture of 0.49 m^2; the solid-angle, main-beam efficiency is 0.9; the operating wavelength is 8 mm.

The flux image was computed from data taken from a public archive.

REFERENCE

1. Stacey, J.M. Target Detection Using Microwave Irradiances From Natural Sources, JPL Publication 84-70, November 1983.

TECHNICAL REPORT STANDARD TITLE PAGE

1. Report No. JPL Publication 85-12	2. Government Accession No.	3. Recipient's Catalog No.
4. Title and Subtitle Microwave Responses of the Western North Atlantic		5. Report Date February 15, 1985 6. Performing Organization Code
7. Author(s) J.M. Stacey		8. Performing Organization Report No.
9. Performing Organization Name and Address JET PROPULSION LABORATORY California Institute of Technology 4800 Oak Grove Drive Pasadena, California 91109		10. Work Unit No. 11. Contract or Grant No. NAS7-918 13. Type of Report and Period Covered JPL Publication
12. Sponsoring Agency Name and Address NATIONAL AERONAUTICS AND SPACE ADMINISTRATION Washington, D.C. 20546		14. Sponsoring Agency Code
15. Supplementary Notes		

16. Abstract

Features and objects in the Western North Atlantic Ocean -- the Eastern Seaboard of the United States -- are observed from Earth orbit by passive microwaves. The intensities of their radiated flux signatures are measured and displayed in color as a microwave flux image.

The features of flux-emitting objects such as the course of the Gulf Stream and the occurrence of cold eddies near the Gulf Stream are identified by contoured patterns of relative flux intensities.

The flux signatures of ships and their wakes are displayed and discussed. Metal data buoys and aircraft are detected.

Signal-to-clutter ratios and probabilities of detection are computed from their measured irradiances. Theoretical models and the range equations that explain passive microwave detection using the irradiances of natural sources are summarized.

17. Key Words (Selected by Author(s))	18. Distribution Statement
Electronics and Electrical Engineering Geosciences and Oceanography (General) Intelligence Navigation, Detection, and Countermeasures (General)	Unlimited/unclassified

19. Security Classif. (of this report)	20. Security Classif. (of this page)	21. No. of Pages	22. Price
Unclassified	Unclassified		